Available online at www.sciencedirect.com

ScienceDirect

journal homepage: www.elsevier.com/locate/he

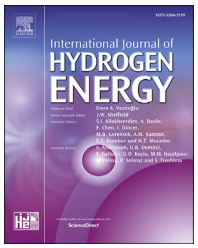

A hybrid 1D-CFD numerical framework for the thermofluidic assessment and design of PEM fuel cell and electrolysers

Joanes Berasategi [a], *Markel Penalba* [a,b,*], *Ricardo Blanco-Aguilera* [a], *Manex Martinez-Agirre* [a], *M. Mounir Bou-Ali* [a], *Valentina Shevtsova* [a,b]

[a] *Fluid Mechanics Department, Mondragon University, Loramendi 4, 20500 Arrasate, Spain*
[b] *Ikerbasque, Basque Foundation for Science, Euskadi Plaza 5, Bilbao, Spain*

ARTICLE INFO

Article history:
Received 28 October 2022
Received in revised form
2 June 2023
Accepted 7 June 2023
Available online 1 July 2023

Keywords:
Hydrogen technologies
Fuel cells & electrolysers
CFD simulations
1D analytical modelling
Hybrid coupling

ABSTRACT

Given the current maturity of hydrogen technologies, accurate and computationally efficient numerical models are crucial for improving their understanding and development. Traditional models are either computationally prohibitive or lack the capacity to assess the spatial distribution of critical variables. The present paper suggests a hybrid numerical model for Fuel Cells (FCs) and electrolysers, articulating the coupling between a 1D analytical model and a Computational Fluid Dynamics (CFD) model via a nonlinear regression. Results present an initial validation of the 1D analytical model and the CFD model, and, once the validation is proven successful, the hybrid model is evaluated with a relatively long and highly varying loading profile that covers a wide range of the potential operational points of a FC. The hybrid model shows promising results, showing fidelity levels similar to CFD models, including the capacity to assess the spatial distribution, and a low computational cost. Hence, this hybrid model is demonstrated to be an attractive tool for the design of FCs and electrolysers, optimisation of thermal management and control strategies, degradation analysis, and techno-economic analysis.

Introduction

The transition towards a zero-emission energy system is one of the most critical actions for the reduction of greenhouse gas emissions, the restriction of global warming below 2 °C and the mitigation of the most dramatic climate change impacts [1]. This transition relays on a massive electrification of the energy system based on the implementation of diverse renewable energy plants (*i.e.* wind, solar, marine energy plants) to replace the currently dominant fossil energy sources. However, the well-known limitations of renewable energy sources, and the particular requirements of certain sectors, such as the transport and mobility sector or the energy-intensive industries, restrict the direct use of renewable electricity. In this context, green hydrogen (H_2) becomes an interesting alternative energy vector for the decarbonisation of these critical sectors [2–4].

* *Corresponding author*. Fluid Mechanics Department, Mondragon University, Loramendi 4, 20500 Arrasate, Spain.
E-mail address: mpenalba@mondragon.edu (M. Penalba).
https://doi.org/10.1016/j.ijhydene.2023.06.082

Hence, a massive implementation of new renewable energy plants and hydrogen technologies will be necessary in the short- and medium-term future [5], for which the latter implies the implementation of infrastructures dedicated to H_2 generation, storage, transport/distribution and conversion. While renewable energy technologies are mature technologies, especially solar and wind, the most promising hydrogen technologies still need a few years of R&D efforts to achieve maturity. Currently, the most critical aspects of the development of hydrogen technologies are H_2 generation and transformation, where the largest R&D efforts are focused on. The former is achieved by water electrolysis and the latter uses fuel cells (FCs), both being similar in terms of construction, manufacturing and operation, although the water electrolysis process is somewhat the inverse of the electricity generation through a FC.

For both processes, there exist technologies that are based on different principles. The three most relevant technologies are (i) alkaline, (ii) Proton-Exchange Membrane (PEM) and (iii) high-temperature solid-oxide electrolysers and FCs. Currently, the alkaline electrolysers and FCs are the most widespread technologies due to their simplicity and maturity [6], meaning that, most likely, alkaline technologies will be implemented in the majority of hydrogen generation and transformation plants in the next years. PEM technologies have demonstrated to significantly improve the performance of alkaline electrolysers and FCs, with considerably higher current density, compactness, operation flexibility, efficiency and better resistance to corrosion [7–10]. However, the lower maturity of PEM solutions results in higher high manufacturing costs and lower expected lifetimes [7], which delays their massive implementation in the next years. Similarly, high-temperature solid-oxide solutions have some advantages against the alkaline and PEM technologies [11], such as higher efficiency and higher stack power (up to 2 MW), but their technology readiness level (TRL) is still relatively low [12]. Other less developed technologies like the anion-exchange membrane are also being studied, but are still in a very low level of development for their consideration as potential future solutions [12].

Among the three main technologies mentioned above, the PEM seems to be the most promising technology due to the trade-off between its level of maturity and performance, resulting in a suitable alternative for a wide range of diverse applications, from automotive to aerospace applications [13]. The main challenges in the development of PEM electrolysis and FC designs are the following.

- the high cost (about 50% higher compared to alkaline [12]),
- Membrane hydration via air and water management [14],
- Temperature management as a large quantity of heat is generated [15], and
- Durability.

Therefore, the present study focuses on PEM technologies, with a special emphasis on the development of numerical tools for their thermal management, although the techniques described in this study are easily applicable to other electrolysis and FC technologies.

In the development process towards higher TRLs, precise numerical models are essential. The literature shows mathematical models based on different principles and assumptions, which can be classified into two main groups [16]: 1D analytical models and 3D computational fluid dynamics (CFD) models. The former are computationally very efficient, but rely on heavy assumptions and restrict the spatial analysis to a single dimension. In contrast, the latter consider all the relevant physical phenomena in all the three dimensions, but result in computationally expensive (almost prohibitive) simulations. Overall, the literature shows that 1D analytical models provide relatively accurate predictions of the optimal operating conditions for fuel cell and electrolysers, and include the capacity to characterise the impact of different physical parameters (*e.g.* membrane humidity, operation pressure and temperature, and hydrogen purity) on the performance. The more precise 3D numerical simulations are reserved for more detailed predictions where the spatial distribution is relevant, as for the design of gas/coolant channels and the study of water saturation effects, for example.

1D analytical models

In general, 1D analytical models are divided in two interconnected parts. On the one hand, the polarisation curve is modelled based on the three main overpotentials (*i.e* activation, ohmnic and mass transfer overpotentials) that are subtracted or added to the ideal voltage in FCs and electrolysers, respectively. Fig. 1 illustrates a characteristic polarisation curve of a FC and the losses due to the different effects. Thus, the operating cell voltage is given as follows,

$$V_{cell} = V_{oc} \pm V_{act} \pm V_{ohm} \pm V_{con}, \quad (1)$$

where V_{oc} is the ideal open-circuit voltage, and V_{act}, V_{ohm} and V_{con} are the activation, ohmnic and concentration overpotentials, respectively. These overpotentials are computed in the anode and the cathode, which are given by means of an analytical formulation.

On the other hand, the hydrogen and water transport through the membrane is computed based on a dynamic

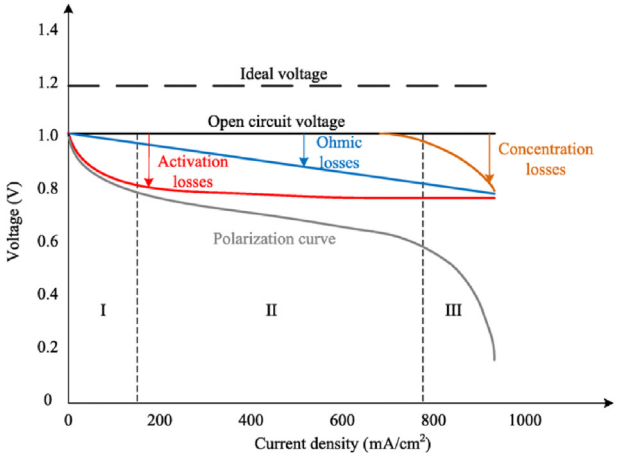

Fig. 1 – Typical polarisation curve of a PEM fuel cell, identifying the different voltage losses [17].

model that is often simulated in the Matlab/Simulink® environment. Commonly, this type of dynamic models consider two main phenomena that drive the water transport through the membrane: electro-osmotic drag and back-diffusion. Electro-osmotic drag is the number of water molecules transported per proton (from the anode to the cathode in FCs and the inverse in electrolysers), while the back-diffusion produces a counter-flow (from the cathode to the anode in FCs and the inverse in electrolysers) due to concentration gradients at both sides of the membrane.

This model structure is used in several different studies in the literature, both in FCs and electrolysers, for which the mathematical models are based on the same equations [8]. In the case of hydrogen FCs, among others [18], presents a dynamic 1D model coded in Matlab for performance evaluation under different operating conditions (*i.e.* relative humidity, temperature, pressure and species concentration) [19], suggests a Matlab/Simulink model with the same purpose [20], uses a 1D model for the optimisation of the air compressor as a function of the pressure ratio and the air-fuel ratio, and [21] studies the sensibility of 1D models to the loss of performance due to degradation effects by comparing different 1D models.

The literature also shows different studies where water electrolysers are analysed via 1D models. For example [22], presents a Matlab/Simulink model for the characterisation of a water electrolyser that includes different balance of plant (BoP) components under a wide range of operating conditions, identifying the losses in each component of the electrolysis system. Similarly [23], suggests a dynamic Matlab/Simulink model calibrated against experimental results, conducting a model parameters identification strategy based on the metaheuristic Particle Swarm Optimisation algorithm. The BoP of FCs and electrolysers is very similar. Hence, dynamic 1D models suggested in the literature are almost identical for FCs and electrolysers. For example [23], presents a 1D dynamic model for an electrolyser that is equivalent to the FC model suggested in Ref. [8].

CFD models

Due to the complexity to obtain high-fidelity results of the water transport dynamics via experimental campaigns, two-phase CFD models for FC and water electrolysers have been developed in the recent years. Two-phase flows in FCs are commonly represented via Volume of Fluid (VOF) models, although the coupling with the electrochemical model may become problematic [14]. One of the pioneering VOF-based simulation for FCs is presented in Ref. [24] which considers unsteady multi-phase phenomena and includes all the main components of a FC (*i.e* the membrane, the catalyst layer (CL), gas channels, the gas diffusion layer (GDL) and current collectors). The first study using this VOF model focuses on the characterisation of the generated current density as a function of the velocity field, pressure, reactants and temperature distributions in a single-serpentine FC. The same model is later employed with the same purpose in multi-serpentine configurations [25], interrelated flow fields [26] and in a three-cell PEM fuel cell stack [27]. Chen et al. [28] presented a similar model based on the Tafel equation [29] for the estimation of the current density, where the behaviour of liquid water in a straight gas channel and its impact on mass transport and current distribution is evaluated for different air inlet velocities and gas channel wall wettability. These and other model presented in the literature are reviewed in Ref. [30]. Finally [31], presents an interesting benchmarking study of CFD models for PEM FCs, carrying out a comparison of CFD codes for a reference geometry and set of input parameters. Similarly to the dynamic 1D models, the analysis of CFD models for PEM FCs and electrolysers use the same VOF approach, include the same main elements (anode, cathode, membrane, etc.), consist of the same geometry, mesh and boundaries, and employ the same solvers. In this sense [32], presents the equivalent PEM electrolyser CFD model to the FC model suggested in Ref. [28].

Hybrid 1D-CFD models

Despite the significant differences between 1D analytical and CFD modelling techniques, the development of PEM technologies requires the combination of both techniques in the different stages of development. Computationally efficient 1D analytical models are crucial for the design of controllers, thermal management algorithms, broad assessment of the performance along the whole operational range and design optimisation; while high-fidelity CFD models provide higher accuracy to validate the configurations optimised based on the 1D analytical model and 3D spatial analysis to enable geometric optimisation of the different components.

An efficient hybridation of the two mathematical models can achieve a numerical framework that is able to provide a higher fidelity and an estimation of the spatial distribution with a low computational cost. This potential hybrid framework would provide the capacity to improve the performance assessment, and design controllers and thermal management algorithms including the 3D performance. Yet, the combination of both models in the literature is scarce, since researchers and developers tend to use only one of the techniques with the assistance of experimental campaigns, and the hybridation attempts presented in the literature do not provide the characteristics mentioned earlier.

For example [33], presents a hybrid 1D-3D model based on the VOF method, where the domain of the anode and the membrane is defined in 1D, and the cathode domain in 3D. Hence, the 3D model in the cathode includes the two-phase flow and all the water dynamics via a multi-fluid saturation model, while the electrochemical reactions and the different overpotentials in the membrane are simplified and computed in 1D. This hybrid model is developed in ANSYS Fluent®, incorporating the 1D model domain via user. defined functions, and the communication between the two domains is conducted by imposing the bottom wall species boundary conditions in the 3D domain. A similar approach is also suggested in Ref. [34] for the analysis of two-phase flow patterns on the FC, where the cathode is modelled via a 3D domain, simplifying the rest of the domain to 1D. However, the VOF model presented in Ref. [34] imposes the water flow entering the gas channels instead of computing the flow as a function of the current density at the FC and the water balance at the membrane is not included. Ding et al. [35] improved their 3D VOF model to incorporate the water flow in each pore as a

function of the water generation rate in the surrounding area, improving the ohmic losses. However, the model still considers the membrane fully hydrated.

Hence, the 1D-CFD hybrid models presented in the literature allow for a 3D spatial analysis only at the cathode and the computational burden of the hybrid model is still significantly high, especially for optimisation purposes. Therefore, this paper presents a novel hybrid 1D-CFD model with the objective of designing the optimal thermal management system. For the sake of simplicity, the present paper focuses on the hybridisation of a hydrogen PEM FC. However, note that due to the similarities between the real PEM FC and electrolyser systems (i.e. both in the cells and the BoP) and their operating principles, the modelling techniques for 1D dynamic models and CFD approaches are almost identical. Therefore, the methodology and numerical frameworks developed in the present study for PEM FCs can be easily transferred to PEM electrolysers.

The paper is organised as follows: Section Fuel cell mathematical modelling describes the analytical 1D and CFD mathematical models for PEM fuel cells used in the present study, Section Model hybridation methodology describes the hybridation process for coupling the 1D and CFD models, Section Case study presents the cases study including the characteristics of the specific FC and the input loads analysed in this study, Section Results presents the most relevant results, and Section Conclusions draws the main conclusions of the study.

Fuel cell mathematical modelling

As described in Section Introduction, the mathematical model of a typical PEM FC is divided into two main parts: the voltage model where the different overpotential mechanisms are defined, and the water transport model in the three main components of a FC (i.e anode, cathode and membrane). This separation appears specially in the case of the 1D analytical model, but also in CFD models, as shown in Sections 1D analytical model and CFD model, respectively.

1D analytical model

The 1D model is comprised of a set of inter-connected analytical equations and dynamic differential equations based on the following assumptions.

- Current is uniformly distributed over the whole surface of the membrane ($I = Ai$, being I the absolute current, A the effective area of the FC and i the current density) and, as a consequence, gases are considered to be at constant pressure and uniformly distributed in the FC, and water activity is uniform across the membrane
- The reactant gases (hydrogen at the anode and oxygen at the cathode) are assumed to be in equilibrium with liquid water
- No pressure gradient exists between the anode and the cathode, meaning that convection is neglected
- Anode, Membrane Electrode Assembly (MEA) and cathode are assumed to be at the same temperature
- No electrical conduction is considered across the PEM membrane.

Since the hydration of the membrane is a key aspect in both parts, voltage and water transport models are tightly linked to the water content in the membrane (λ), which is given as a function of the water activity (a), which is commonly defined as the combination of the relative humidity (RH) and the liquid water volume fraction s [36]: $a = RH + 2s$. In Nafion® membranes, the water content is empirically described as [36],

$$\lambda = \begin{cases} 0.043 + 17.81a - 39.85a^2 + 36a^3 & a \leq 1 \\ 14 + 1.4(a-1) & 1 < a < 3 \end{cases} \quad (2)$$

It should be noted that Equation (2) was derived for a Nafion® membrane at 30 °C. Yet, Equation (2) has been shown to be valid also for higher temperatures.

Voltage model

The voltage model in the 1D analytical model follows the superposition described in Equation (1), where, in the case of a PEM FC, the sum of the different overpotentials result in a voltage loss with respect to the initial open-circuit ideal voltage. These overpotentials arise due to activation reactions in the catalyst layers, and the migration of electrons in the bipolar plates and the PEM. Conventional catalyst layers are made of platinum dispersed on a carbon support, which enables splitting hydrogen molecules at the anode and the oxygen reduction in the cathode. Therefore, platinum catalysts are also considered in the present study.

Open-circuit voltage. The open-circuit cell voltage is the ideal voltage achieved by the cell at the thermodynamic equilibrium, commonly represented by a modified form of the Nerst equation as follows,

$$V_{oc} = V_{rev} + \frac{RT}{2F}\ln(p_{H_2}\sqrt{p_{O_2}}), \quad (3)$$

where V_{rev} the reversible voltage that is sensible to temperature variations with respect to a reference temperature (T_{ref}) [37],

$$V_{rev} = V^0_{rev} + (T - T_{ref})\frac{\Delta S}{nF}, \quad (4)$$

$V^0_{rev} = 1.229$ V is the minimum theoretical voltage, R is the universal constant for ideal gases, F the Faraday constant, T the temperature of the cell, n the number of electrons involved in the process, ΔS the standard entropy change, and p_{H_2} and p_{O_2} are the partial pressures of the species. Other similar equations are also suggested in Ref. [18], where the partial pressure of water (p_{H_2O}) is also included. In addition, empirical functions have also been suggested for the determination of V_{oc} as a function of the cell temperature and partial pressures of the species [38].

Activation overvoltage. The activation overvoltage arises because the transfer between the electrolyte and the electrode (or *vice-versa*) is limited by the activation energy barrier. The probability of exciting up to the transition state is proportional to the attempt rate and an exponential distribution of the effective barrier and the temperature. In addition, the reactant consumption and the speed of the electrochemical reaction are proportional to the surface concentration and the

electrical current, respectively. Thus, following the Butler-Volmer equation, the activation overpotential in the anode and the cathode at equilibrium are given as follow [19],

$$V_{act}^{an} = \frac{RT}{\alpha_{an} F} \ln\left(\frac{i}{i_0^{an}}\right), \tag{5}$$

$$V_{act}^{cat} = \frac{RT}{\alpha_{cat} F} \ln\left(\frac{i}{i_0^{cat}}\right), \tag{6}$$

where i_0 is the exchange current density of a platinum electrode and is given as a function of a reference value $i_{0,ref}$ [38], being α the charge transfer coefficient, L the platinum catalyst loading, p the partial pressure of the corresponding specie (*i.e* H_2 in the anode and O_2 in the cathode for a FC) and ΔG the variation in Gibbs free energy. The water activity is further defined later in Section Water transport model, where the function for the determination of water content (λ) inside a PEM membrane is described.

$$i_0^{an} = i_0^{cat} = i_{0,ref}\, a\, L \left(\frac{p}{p_{ref}}\right) \exp\left[-\frac{\Delta G}{RT}\left(1 - \frac{T}{T_{ref}}\right)\right], \tag{7}$$

Ohmic overvoltage. The ohmic overvoltage arises due to two main factors: electrical resistance in electrical components and the ionic resistance due to the proton flow through the membrane. The ionic resistance is the most dominant factors and, as a consequence, most of the models neglect the electrical resistance. Therefore, the overpotential can be determined as follows,

$$V_{ohm} = \frac{i\, \delta_{mem}}{\sigma_{mem}}, \tag{8}$$

where, δ_{mem} and σ_{mem} are the PEM membrane thickness and conductivity, respectively. The former is a geometrical parameter and the latter is expressed empirically as [36],

$$\sigma_{mem} = (0.005139\lambda - 0.00326) \exp\left[\frac{-\Delta G}{R}\left(\frac{1}{T_{ref}} - \frac{1}{T}\right)\right], \tag{9}$$

where $\frac{-\Delta G}{R} = 1268$ K and $T_{ref} = 303$ K.

Concentration overvoltage. The concentration overvoltage becomes relevant only at high current density rates (between 500 and 1500 mA/cm^2 [39]) due to oxygen bubbles covering the membrane surface that limit the hydrogen supply hindering the electrochemical reaction [40]. Hence, the concentration overpotential in the anode and cathode is defined as a function of a limiting current density (i_L) as follows [38],

$$V_{con} = \frac{RT}{nF} \ln\left(\frac{i_L}{i_L - i}\right), \tag{10}$$

where,

$$i_L = \frac{n\, F\, D\, C}{\delta_e}, \tag{11}$$

and D is the diffusion coefficient of the gas mixture, C the molar concentration and δ_e the electrode thickness. The diffusion coefficient is also defined empirically [41,42] as a function of a reference diffusion parameter (D_{ref}), adjusting the diffusion coefficient for the corresponding electrode porosity (ε) and tortuosity (τ), and s, being $T_{ref} = 353.15$ K and $p_{ref} = 1$ atm.

$$D = \frac{\varepsilon}{\tau^2}(1 - s)^3 D_{ref} \left(\frac{T}{T_{ref}}\right)^{1.5} \frac{p_{ref}}{p}, \tag{12}$$

Water transport model

Due to the assumptions described above, water transport is only considered due to electro-osmotic drag ($\dot{N}_{H_2O}^{eod}$) and back-diffusion ($\dot{N}_{H_2O}^{bd}$), neglecting hydraulic pressure and thermo-osmotic phenomena [43]:

$$\dot{N}_{H_2O}^{mem} = \dot{N}_{H_2O}^{eod} - \dot{N}_{H_2O}^{bd}. \tag{13}$$

Electro-osmotic drag. arises due to the attraction of polar water molecules to the protons that travel from the anode to the cathode. Hence, the molar transport due to the electro-osmotic drag is defined as follows,

$$\dot{N}_{H_2O}^{eod} = n_d \frac{i}{F}, \tag{14}$$

where n_d is the electro-osmotic drag coefficient that is empirically defined as a function of the PEM membrane water content [43],

$$n_d = 2.5 \frac{\lambda}{22}. \tag{15}$$

Note that other alternatives defined via different empirical equations based on λ are also suggested in the literature [44].

Back-diffusion. generates a water flow in the opposite direction (from the cathode to the anode), partially compensating the water loss in the anode. The molar flow for back-diffusion effects is given as follows based on Fick's law,

$$\dot{N}_{H_2O}^{bd} = \frac{A D_w}{\delta_{mem}} \left[C_{H_2O,mem}^{cat} - C_{H_2O,mem}^{an}\right], \tag{16}$$

where D_w is the diffusion coefficient, and $C_{H_2O,mem}^{cat}$ and $C_{H_2O,mem}^{an}$ the water concentrations in the cathode and the anode, respectively. The latter diffusion coefficients in the different 1D analytical models are defined either following theoretical expressions for the Knudsen and binary diffusion phenomena [19], or an empirical equation as a function of water content [45]. The model presented in this paper used the former.

Power output and heat transfer

Finally, as the main outputs of the FC, the performance of the FC can be computed by means of cell power output (P_{cell}), heat flow (Q_{cell}) and efficiency (η_{cell}), which are defines as follows,

$$P_{cell} = I V_{cell}, \tag{17}$$

$$\eta_{cell} = \frac{V_{cell}}{V_{LHV}}, \tag{18}$$

where V_{LHV} is the lower heating values of hydrogen ($V_{LHV} = 1.254$ V [38]). From the FC outputs, the computation of stack outputs is straightforward, assuming that all the losses in the power production process are dissipated in the form of heat,

$$P_{stack} = N_{cell} I V_{cell}, \tag{19}$$

$$Q_{cell} = \left(\frac{P_{stack}}{\eta_{cell}}\right) - P_{stack}, \tag{20}$$

where N_{cell} is the number of cell in the stack.

CFD model

The CFD model employed in this study is a 3D model that articulates the most relevant effects and phenomena that can affect the performance of a fuel cell: (i) transport analysis to model the transfer of different species in the membrane, the GDL and flow channels, (ii) the electrochemical analysis in the membrane to estimate the voltage level at which the FC operates under different thermofluidic and electric load conditions, and (iii) thermal analysis for the assessment of the temperature distribution over the FC and the heat losses. Hence, the CFD model is built upon the following assumption.

- Steady-state (no transient response is included),
- Laminar flow regime of the reactant gases,
- Gases behave as ideal gas,
- All water exists as gas, and no phase change is considered,
- All porous layers (*i.e.* GDLs, CLs and membrane) are considered isotropic, and
- Thermo-physical properties of the 3D model are constant.

Based on these assumptions, the following governing equations form the CFD model, using the Navier-Stokes equations as the basis: continuity, momentum, mass transport (also known as species conservation) and energy equations describe the transport of species in the model. In contrast, the charge conservation equation models the electrochemical reactions within the FC, which occurs exclusively at the CL. This equation is divided into electric and protonic transport equations.

The continuity equation, in its broadest form, is given as,

$$\frac{\partial(\rho u)}{\partial x} + \frac{\partial(\rho v)}{\partial y} + \partial(\rho w)\partial z = -\frac{\partial \rho}{\partial t} \tag{21}$$

where u, v and w are the velocity of reactant gases in x, y and z directions, respectively, while ρ is the density of these gases. If Equation (21) is adapted for porous elements, such as electrodes and membranes, and ε is considered the porosity of these elements, continuity equation yields,

$$\frac{\partial(\rho\varepsilon u)}{\partial x} + \frac{\partial(\rho\varepsilon v)}{\partial y} + \frac{\partial(\rho\varepsilon w)}{\partial z} = S_m \tag{22}$$

where S_m is the mass sink that represents the variation of the reactants due to chemical reactions. However, no reactions exist in the flow channels and the GDL, meaning that this term is neglected. This sink term is only considered in the CL, where reactions of the reactants are expected.

Similarly, the generic momentum equation must be adapted to a porous context including ε as follows,

$$\nabla\cdot(\varepsilon\rho\vec{v}\vec{v}) = -\varepsilon\nabla p + \nabla\varepsilon\tau + S_{mom} \tag{23}$$

where $\vec{v}$ represents the velocity vector, p is the pressure, τ the shear tensor and S_{mom} the momentum sink term. The sink term is also assumed zero in the flow channels, and

$$S_{mom} = -\frac{\mu u}{\beta} \tag{24}$$

in the rest of the porous layers of the FC, being μ the dynamic viscosity of the reactant and β the permeability.

The diffusion phenomena is one of the most relevant effects for the transport of reactants in FCs and is considered in the mass transfer equation, which, for the case of porous elements, is given described as,

$$\nabla(\rho\varepsilon\vec{v}y_i) = \nabla\left(\rho\varepsilon D_{ij}^{eff}\nabla y_i\right) + S_{m_i} \tag{25}$$

where D_{ij}^{eff} is the diffusivity of the specie i inside j, and y_i represents the mass fraction. Likewise the continuity equation, the sink term is assumed to be zero in the flow channels and GDLs due to non-reactive flows, while must be considered in the CL.

The last equation for adequately capturing the mass transfer of species in the different layers of a FC is the energy equation, which is given as,

$$\nabla(\vec{v}(\rho + P)) = \nabla\left(k_{eff}\nabla T - \sum h_j\vec{J_j} + (\tau_{eff}\vec{v})\right) + S_h, \tag{26}$$

where h is the enthalpy, τ_{eff} the effective shear tensor, k_{eff} the effective conductivity, $\vec{J_j}$ the mass flux vector and S_h the energy sink term.

Once the mathematical framework of the mass transfer within the CFD model is fully described, the charge conservation equation that characterises the electrochemical reactions within the FC is described as a combination of the following two equations:

$$\nabla(\sigma_{eff}\nabla\phi) + R = 0, \tag{27}$$

where σ_{eff} is the effective conductivity that varies as a function of the water content as illustrated in Equation (9), and ϕ the potential. Note that Equation (27) can be use for characterising, both protonic and ionic potentials, just by applying the corresponding conductivity.

In order to solve these equations, the definition of boundary conditions, and a geometry and its discretisation are vital. The implemented boundary conditions are presented in Table 1, where the subscripts $_{cat}$ and $_{an}$ represent the variables of the cathode and the anode, respectively, and subscripts $_{ion}$ and $_{elec}$ the variables corresponding to the ionic of electric potential equations.

For the study of the FC performance, the CFD model described in Equation 22–27 requires a precisely defined and adequately discretised 3D geometry. On its highest level, this geometry includes the anode, the MEA and the cathode, but both the anode and cathode are, in turn, divided into the current collector, the GDL, the micro-porous layer (MPL) and the CL. Each of these sections is defined with a specific thickness, porosity, permeability and contact angle characteristics in

Table 1 – Boundary conditions for the 3D CFD model for FCs.

Area of application	Boundary conditions
Inlet flow channel (anode)	$y_{H_2} = y_{H_2,in}$ $y_{H_2O} = y_{H_2O,in}$ $T_{in,an} = T_{H_2,an}$ $m = m_{in,an}$
Inlet flow channel (cathode)	$y_{O_2} = y_{O_2,in}$ $y_{H_2O} = y_{H_2O,in}$ $T_{in,cat} = T_{O_2,cat}$ $m = m_{in,cat}$
Outlet flow channel	$\frac{\partial \phi}{\partial z} = 0$
Anode terminal	$\phi_{elec} = 0$ $\frac{\partial \phi_{ion}}{\partial y} = 0$
Cathode terminal	$\phi_{elec} = V_{cell}$ $\frac{\partial \phi_{ion}}{\partial y} = 0$
External boundaries	$\frac{\partial \phi_{ion}}{\partial x} = \frac{\partial \phi_{ion}}{\partial z} = 0$ $\frac{\partial \phi_{elec}}{\partial x} = \frac{\partial \phi_{elec}}{\partial z} = 0$

order to appropriately model the transport of the different species and water. Furthermore, a meticulous discretisation of the geometry is crucial. In the case of the MEA, given the scales of the different layers that form the MEA, the size of the cells is reduced significantly in order to consider a minimum of three layers of cells in each element. For more details about the specifics of the geometry and its discretisation, the readers are referred to Section Case study.

Model verification/validation

The validation of the complete hybrid model is unfeasible due to the lack of a case study in the literature that defines all the required parameters for both the 1D and CFD models In order to provide confidence on the 1D-CFD hybrid model and due to the complexity of validating the hybrid model, each of the models coupled in the hybrid model are validated separately. To that end, the models described in Sections 1D analytical model and CFD model are, respectively, verified and validated against other numerical and experimental results presented in the literature. For verification and validation purposes, the 1D and CFD models have been adapted for the case studies presented in each reference study. Note that, these case studies are different from the one described in Section Case study and, thus, results will also be different.

In the case of the 1D model, the verification exercise focuses on the reproduction of the polarisation curve and aims at demonstrating the sensitivity of the model to the operational conditions under which the FC can work. The verification is carried out against the results presented in Ref. [18], where the response of a FC to a broad variety of different conditions (*e.g.* FC temperature, pressure, RH and O_2 concentration) is presented. The main input parameters of reference 1D model are given in Table A.3 in Appendix A. Fig. 2 illustrates the comparison between the two sets of results, showing a very good agreement for all the different operational conditions. The reference conditions of the cell in Fig. 2 (referred to as REF) correspond to $T = 70\ ^\circ C$, $p = 1.013$ bar, $RH = 96\%$ and $O_2^{con} = 1.2 \times 10^{-6}$.

In contrast, for the 3D CFD model, the validation is carried out against experimental results recently presented in Ref. [46], where the authors used the same set of experimental results for the validation of their CFD model. The main input parameters of the reference CFD model are given in Table A.4 in Appendix A. First, a mesh convergence analysis is carried out in order to ensure that the most relevant dynamics are adequately captured. Likewise the reference study [46], the final mesh consists of 4.1 million elements, guarantying that three elements are included per layer (*i.e.* GDL, MPL, CL and the membrane itself), as illustrated in Fig. 3, with a minimum orthogonal quality of 1.

Fig. 4 compares the polarisation curve obtained via the CFD model described in Section CFD model against the experimental polarisation curve provided in Ref. [46]. The agreement between both curves is also very good, with slight deviations observed in the central part of the curve, where the CFD model seems to underestimate the voltage. However, it is important to note that the CFD model developed by the authors of the original work also shows similar deviations, although their model seems to overestimate the voltage and the deviations appear at high current densities [46]. In any case, the agreement shown in Fig. 4 is believed to be sufficient and, thus, the CFD model is considered validated.

Model hybridation methodology

Once the two model to be coupled in the hybrid model are validated separately, it is expected that the hybrid model will also provide results that are as accurate, but with a significantly reduced computational time, which is the main objective of the present study. Each model is implemented in a different software, *i.e.* the 1D model is implemented in Matlab/Simulink and the CFD model in ANSYS Fluent, which can enhance the complexity of the coupling. However, the approach used in the present study only considers a one-way coupling, meaning that the two software do not need to communicate with each other iteratively, but transmit the information in a hierarchical way. This significantly reduced, both the complexity of the coupling and the computational cost.

Fig. 5 presents the framework of the hierarchical coupling between the two models, where the coupling is shown to be effectively expressed via the nonlinear regression model. In general, hierarchical coupling strategies enable, on the one hand, the use of results from the different layers of the model, and, on the other, the combination of these results from the individual models into a self-consistent non-intrusive coupling. That way, the functionality of the underlying individual numerical models remains unaffected by the coupling. In the present study, the hierarchical hybridation approach enables the use of information from the different layers and the complete model: (i) The 1D model can provide the evolution of the global electrical (FC current $I_{FC}(t)$ and voltage $V_{FC}(t)$) and thermal parameters (FC temperature T_{FC}), (ii) the CFD models provides the *static* distributions of the different variables (H_2 concentration $H_{2_{cell}}(x,y)$, O_2 concentration $O_{2_{cell}}(x,y)$, temperature $T_{cell}(x, y)$, current density $i_{cell}(x, y)$ and water content $\lambda_{cell}(x, y)$), and (iii)

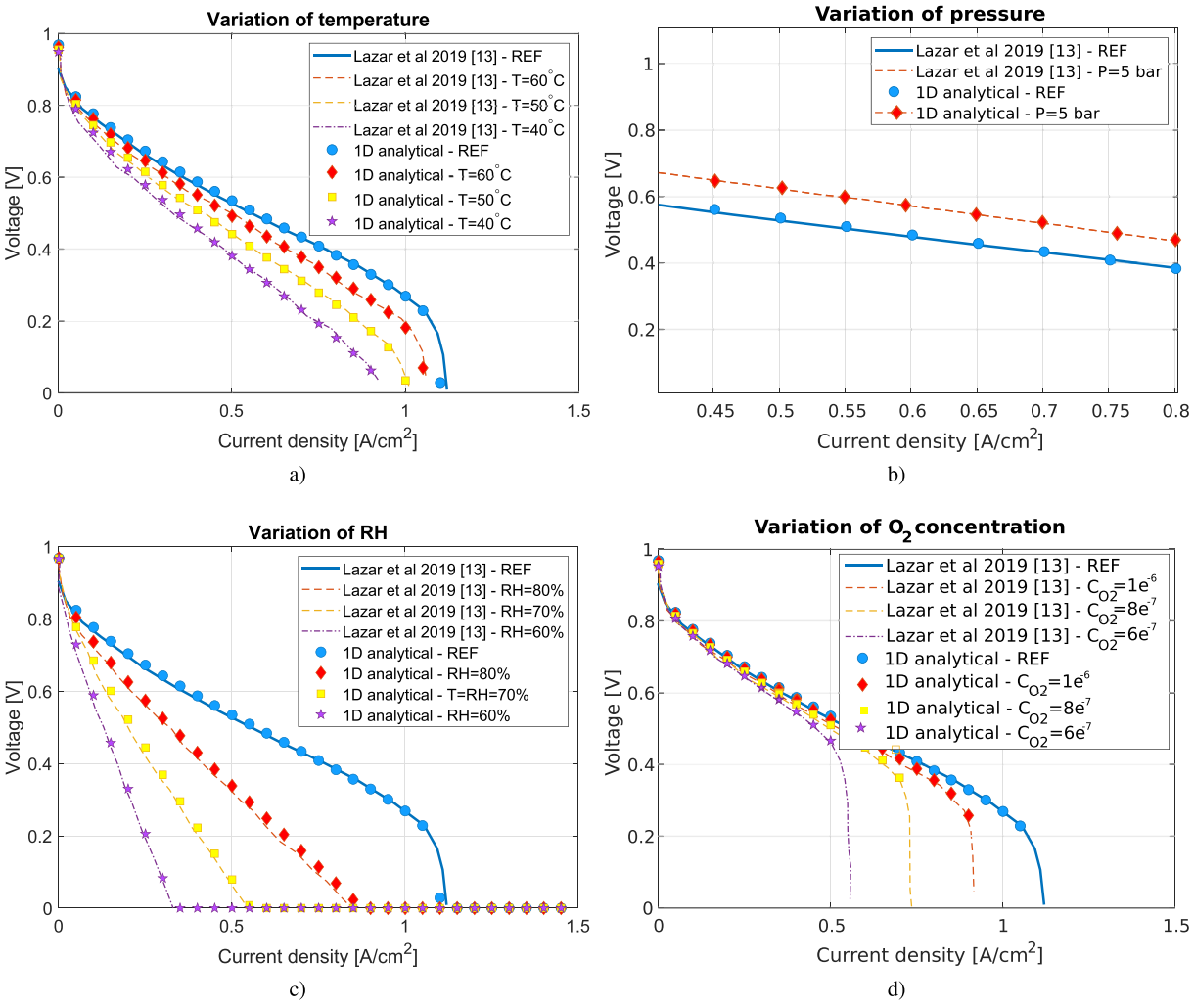

Fig. 2 – Verification of the 1D model against the results shown in Ref. [18]: (a) varies the temperature, (b) the pressure, (c) the RH and (d) the oxygen concentration.

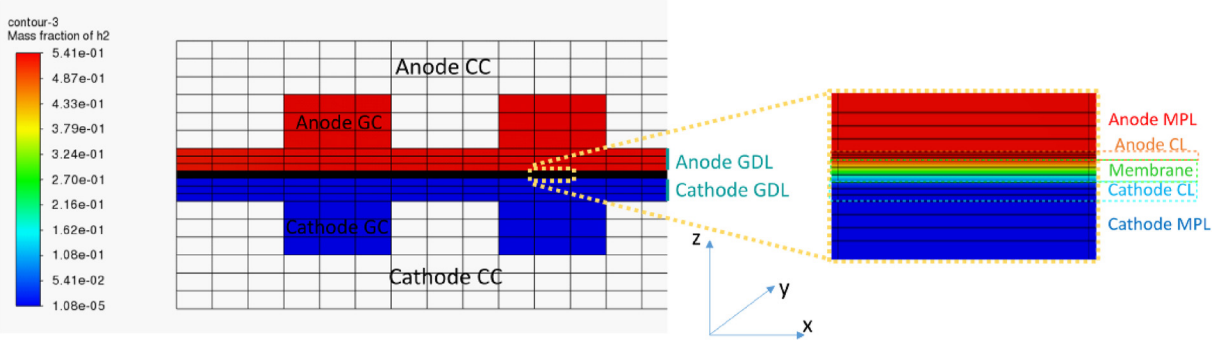

Fig. 3 – Schematic illustration of the mesh designed for the CFD simulations, representing the cross section for the gas channels (GCs), current collectors (CCs) and MEA. Note that the reference dimension of the cells in the longitudinal (x) direction is 0.4 mm.

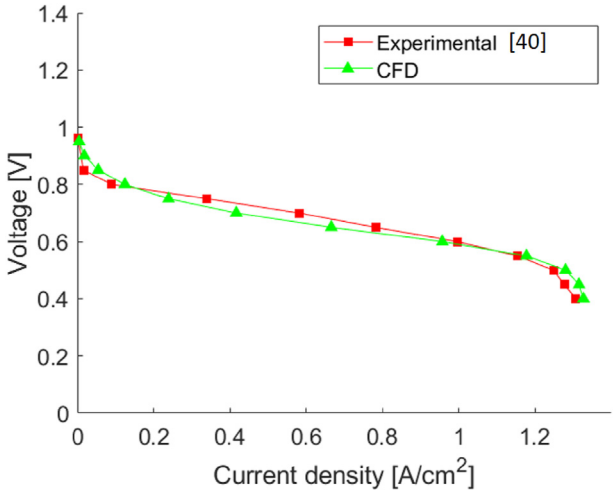

Fig. 4 – Validation of the CFD model against the experimental results presented in Ref. [46].

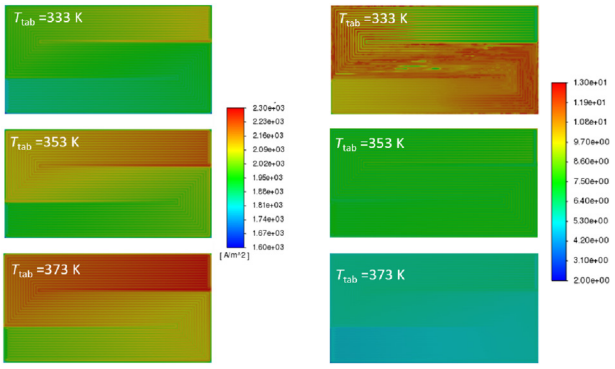

Fig. 6 – Example of a set of *static* CFD results used for the identification of the nonlinear regression model: (left) distribution of current, i, at V = 0.75 V and (right) water content distribution, λ, at V = 0.6 V for different cell temperatures.

the coupling combines the capacities of the two approaches to provide the evolution of the distributions ($H_{2_{cell}}(x,y,t)$, $O_{2_{cell}}(x,y,t)$, $T_{cell}(x,y,t)$, $i_{cell}(x,y,t)$ and $\lambda_{cell}(x,y,t)$). These type of hierarchical approaches are particularly useful for the understanding of multiparameter problems and enables the development of computationally efficient tools.

Thus, the key aspect of the coupling is the nonlinear regression model, which is identified by using a broad range of different operational conditions in CFD. More specifically, the *static* distributions of the main output parameters of the CFD model, under different loading conditions, have been used for fitting the regression model. Fig. 6 depicts some examples of the data used for fitting the model, where the distributions of $i_{cell}(x,y)$ (left) and $\lambda_{cell}(x,y)$ (right) are shown for three different reference temperatures.

These results demonstrate the high sensitivity of the variables to the different operational conditions and the heterogeneous distributions of these variables over the FC. For example, the variation in i_{cell} is significantly higher at the inlet as the FC temperature increases, while the opposite happens with the λ_{cell}. The regression model should be able to reproduce similar patterns in a computationally efficient manner.

Case study

The analysis of the performance of any specific FC is beyond the scope of this paper, so the hybrid 1D-CFD model defined in Section Model hybridation methodology is evaluated on a standard PEM FC, similar to the FCs used in different studies in the literature. In addition, no special attention is paid to the usual FC performance metrics, but the sensitivity of the hybrid model is studied as a response of a dynamic input load. Section Fuel cell definition presents the most relevant characteristics of the FC under study, while Section Loading profiles describes the dynamic input load profiles used in the case study.

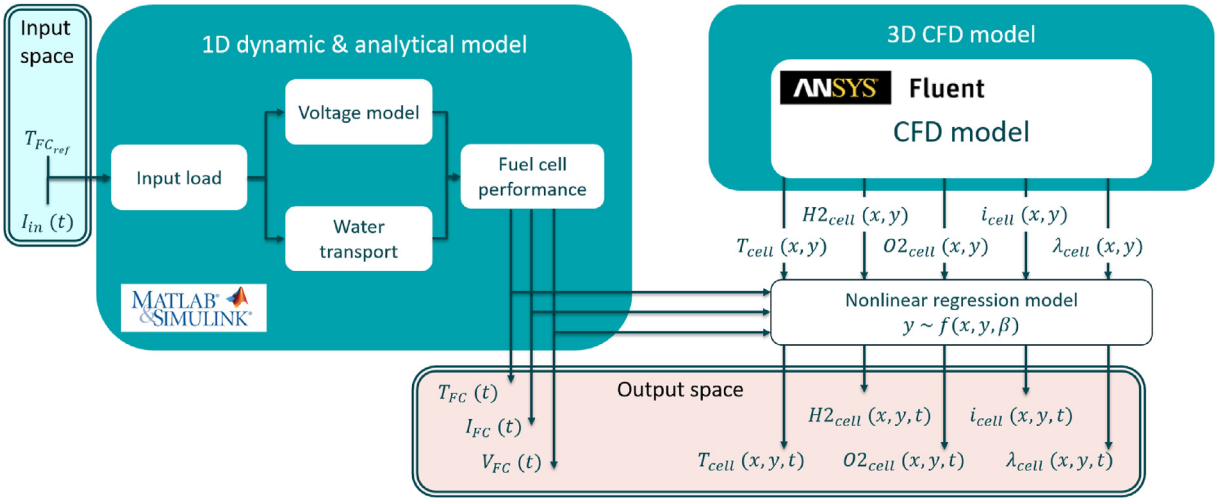

Fig. 5 – Schematic illustration of the hybridation process coupling the 1D model implemented in Matlab/Simulink and the CFD model implemented in ANSYS.

Fuel cell definition

The selected FC is a 100 kW PEM FC composed of 400 cells, each of which has an approximate nominal power of 250 W and an effective area of 200 cm^2. In addition, a flow field design based on a 14-channel-serpentine with crossed reactive flow is implemented. The main geometrical parameters of the FC and the most relevant parameters of the MEA are shown in Fig. 7 and Table 2, respectively.

Loading profiles

For the assessment of the hybrid model, dynamic profiles of the main input variables are designed. These main input variables correspond to the reference temperature profile ($T_{FC_{ref}}(t)$) and the input current profile ($I_{in}(t)$), as defined in the input space in Fig. 5. In order to enable a comprehensive analysis, two relative long (+40 min of duration) and significantly varying profiles are designed, the combination of which covers a wide range of the potential operational conditions of FCs. Note that the input profiles do not correspond to any realistic application, but are simply defined to evaluate the sensitivity of the model to different input conditions. Fig. 8 illustrates the two input profiles, where the combination of both profiles leads to different operational conditions under which the FC will be assessed via the hybrid model. For the sake of clarity when showing the results, three different operational points (OPs) are selected, as shown in Fig. 8.

- i) Medium-performance OP (30 kW - 60 °C),
- ii) High-performance OP (80 kW - 80 °C),
- iii) Low-performance OP (10 kW - 45 °C),

The performance of the FC under these three OPs will be assessed in Section Results.

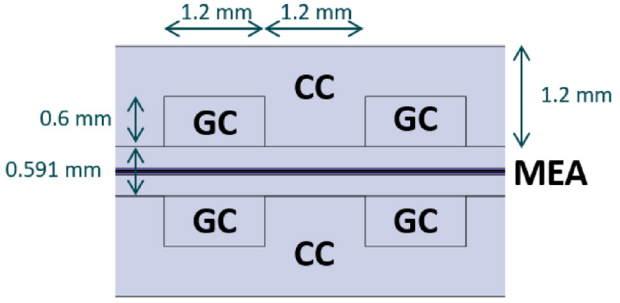

Fig. 7 – Illustration of the FC configuration and its main geometrical characteristics of the cross section for the GC, CCs and MEA.

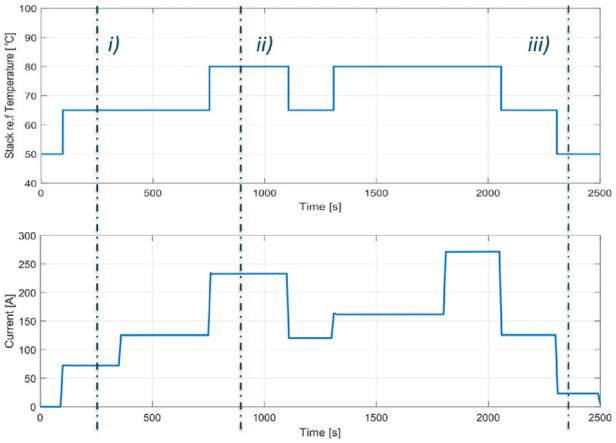

Fig. 8 – Input loading profiles for the assessment of the hybrid 1D-CFD model: (top) reference temperature and (bottom) input current.

Results

As described in Section Hybrid 1D-CFD models, the hierarchical model coupling enables using the information from the different layers of the coupled model, which in this case is particularly interesting. Therefore, in this section, the outcomes of the pure 1D model are analysed first, which are later combined with the outcomes of the hybrid model.

In this sense, Fig. 9 shows the main outcomes of the 1D model, where the overall dynamic response of the FC as a response to the input profiles can be observed, including the electrochemic and thermodynamic response. The voltage and power levels corresponding to each input condition are represented in the two top charts in Fig. 9, including the heat loss of the FC. The two bottom plots in Fig. 9 illustrate the temperature of the FC and the concentration of the different species. Results demonstrate that all the output variables in the 1D model are sensitive to the variations in the input profile. However, this model can only provide the overall information of the FC, meaning that the model simplifies the system to a single point and provide the results corresponding to that point. In fact, from the CFD analysis carried out in Section CFD model and other studies in the literature, it is well known that representation of the system is inaccurate and that each of the variables shown in Fig. 9 do not remain constant over the area of the FC.

This is exactly the information that the hybrid model can provide. For each point of the simulation, the hybrid model can provide the distribution of each variable over the whole

Table 2 – Main characteristics of the MEA of the FC under analysis.

	Anode			Membrane	Cathode		
— —	GDL	MPL	CL		CL	MPL	CL
Thickness [μm]	255	25	5	14	12	25	255
Porosity [–]	0.7	0.6	0.5	–	0.5	0.6	0.7
Permeability [m^2]	3×10^{-12}	1×10^{-12}	2×10^{-13}	1×10^{-18}	2×10^{-13}	1×10^{-12}	3×10^{-12}
Contact angle (°)	110	130	95	–	95	130	110

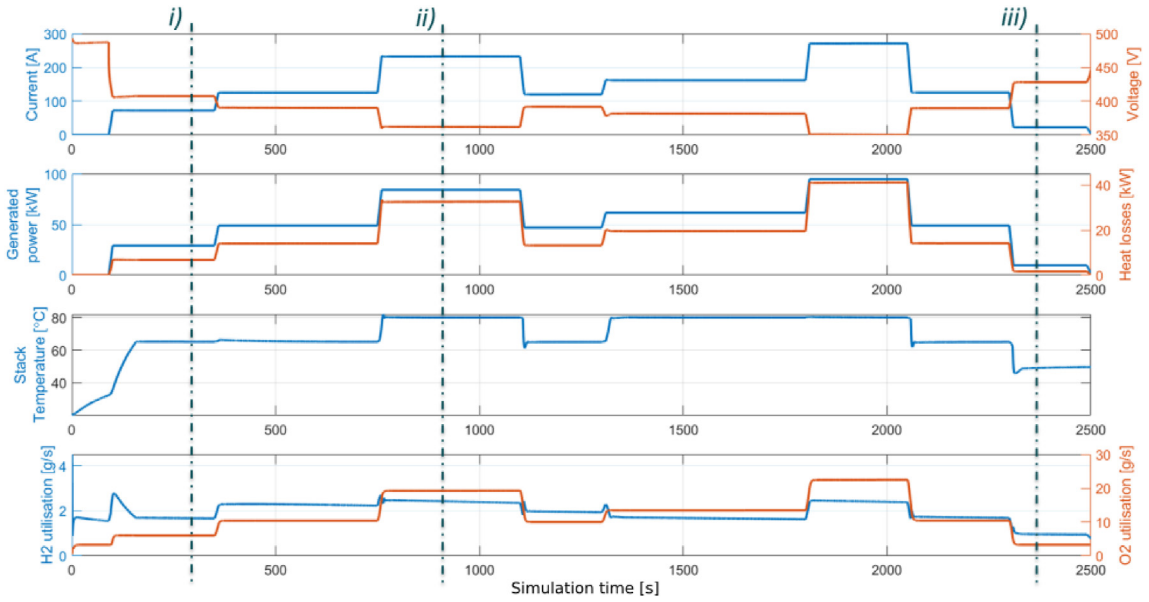

Fig. 9 – Outputs of the 1D model with the three specific operation points highlithed.

area of the FC. As an example of the capacity of the hybrid model, the distribution of the main output variables (*i.e.* λ_{cell}, T_{cell}, i_{cell}, $H_{2_{cell}}$, $O_{2_{cell}}$) for the high-performance operation point is shown in Fig. 10. Results show significant variations across the area of the cell, meaning that the results from the 1D model cannot provide the full picture of the FC's performance, which may lead to inaccurate conclusions. It is interesting to note that the distribution of H_2 and λ seem to be the most varying parameters, although i also varies significantly. In contrast, T_{cell} and $O_{2_{cell}}$ show low spatial gradients. In the case of the temperature, the variation across the cell is low due to the ideal thermal management system implemented in this specific case study, meaning that the reference temperature defined as the input T_{ref} is achieved across the whole cell. With respect to the O_2 concentration, it should be noted that the distributions shown in Fig. 10 represent the section at the anode side of the cell, where the O_2 concentration variations are negligible. for the same reason, H_2 concentration variation is shown to be significant. In any case, each variable shows a different trend for the distribution, which is important to further understand for the understanding of the overall performance of the FC.

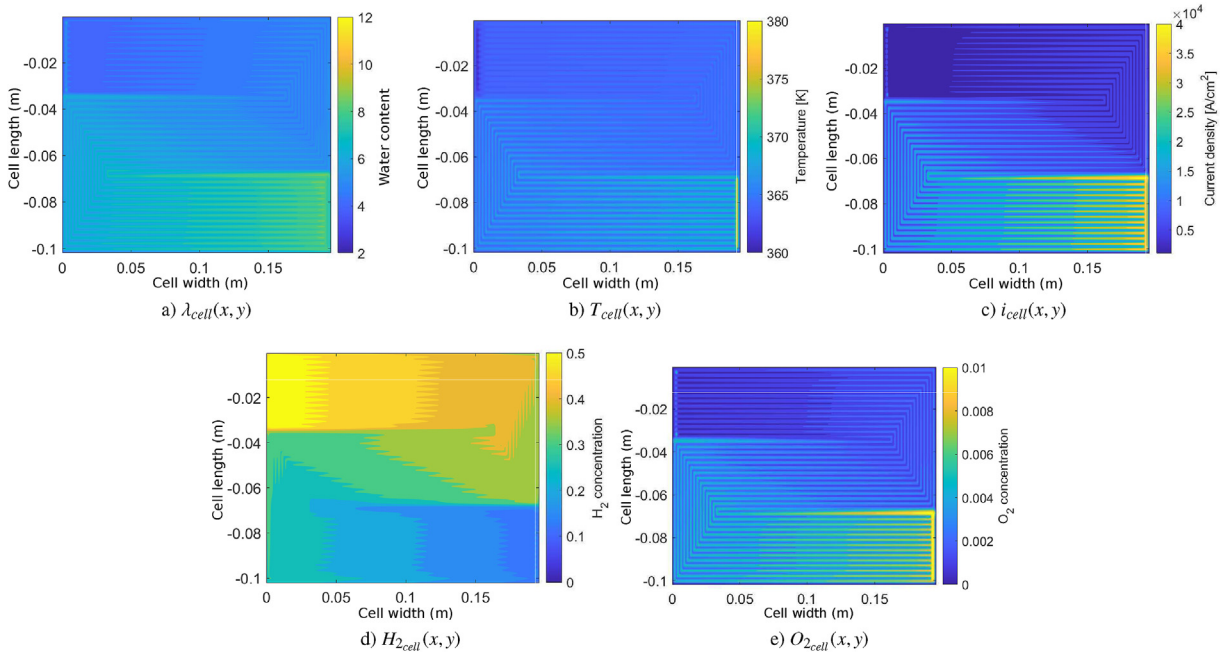

Fig. 10 – Spatial distribution of the most relevant variables at the high-performance operation point.

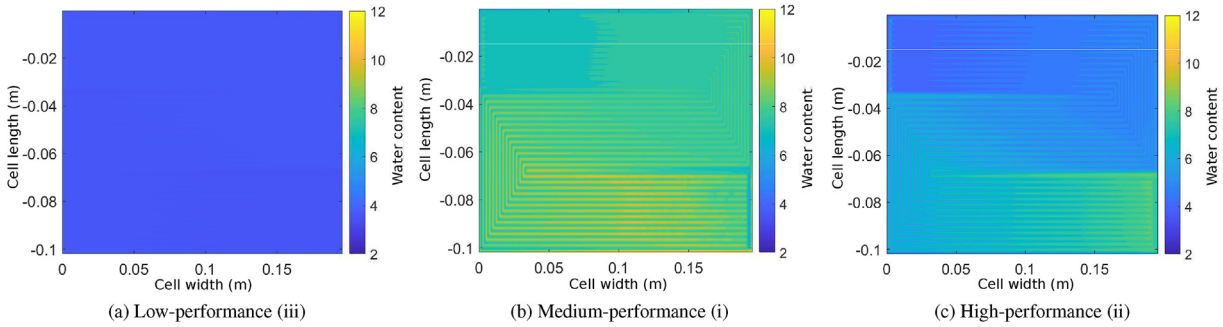

Fig. 11 – Spatial water content distribution $\lambda_{cell}(x, y)$: (a) Low-power, (b) medium-power and (c) high-power.

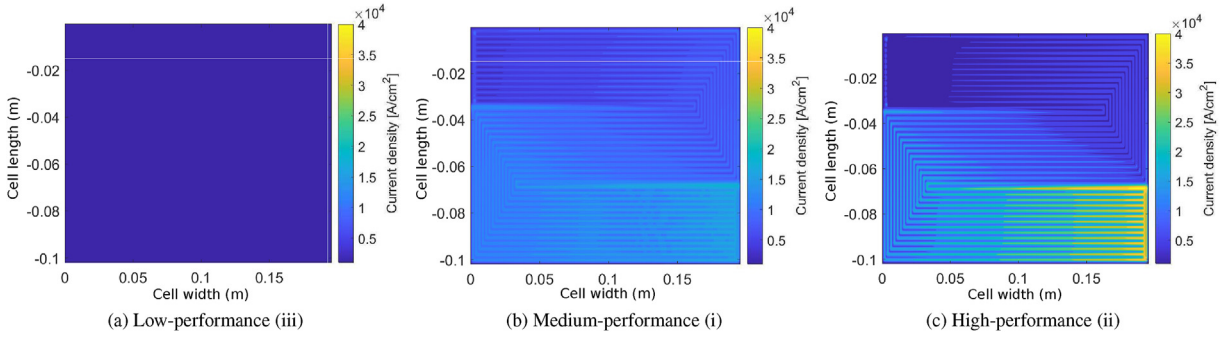

Fig. 12 – Spatial distribution of current density $i_{cell}(x, y)$: (a) Low-power, (b) medium-power and (c) high-power.

To that end, the evolution of these parameters is further analysed in the present study. For the sake of clarity, only two parameters, *i.e.* λ and i, and three points along the simulation, *i.e.* the previously defined low-, medium- and high-performance operation points, are selected for the deeper analysis. Fig. 11 illustrates the variation of λ for the three OPs using the same scale for the three graphs, which enables an easier comparison. However, differences are seen clearly, increasing λ in the system in one order of magnitude between the different OPs and showing differences of up to two- and threefold between the inlet and the outlet of the FC for the same OP. The latter is the type of information the 1D model can never provide due to the assumptions upon which the model is designed. Similarly, Fig. 12 illustrates the same results for i, where one order of magnitude of difference is also shown between the different OPs, but the current density is shown to multiply by 4 and 5 between the inlet and outlet.

This results show the importance of accurately studying the spatial distribution of the most relevant variables, as the input load varies. In fact, the variation of the input load in FCs, with a dynamic behaviour similar to that shown in Fig. 8, may be a common practice in certain applications, where the analysis of the spatial distribution may be crucial in order to better understand the behaviour of the FC, including the performance and the degradation effects. In fact, it is well known that the latter is a local effect, meaning that the understanding of the local behaviour of the FC is vital. In addition, it is important to note that including the regression model barely adds any extra computational cost, meaning that the high-fidelity results with dynamic spatial distributions can be obtained for the same computational cost required by the 1D model, which is a tiny fraction of the CFD burden.

Conclusions

This paper presents a novel hybrid simulation tool that couples a 1D analytical model and a 3D model based on Computational Fluid Dynamics (CFD) for assessing the performance of fuel cells (FCs). The two models are combined by means of a hierarchical coupling approach that enables the use of all the information from the different layers of the hybrid model. The coupling is effectively carried out via a nonlinear regression model fitted based on the results obtained from the pure CFD model. Hence, the hybrid simulation tool can provide the dynamical behaviour of the FC, including the dynamic distribution of the different variables across the geometry of the FC.

Firstly, 1D and CFD models are validated separately against other numerical and experimental results presented in the literature. Then, the capacity of the hybrid model is demonstrated, showing that it can provide high-fidelity results of the dynamic spatial distributions for different variables under diverse operational conditions. These differences are shown to be considerable: up to an order of magnitude of difference between the different operational points, and multiplying factor of up to 5 between the inlet and the outlet at the same operational point. For the computation of these results with the dynamic spatial distributions, the computational cost of the hybrid model is seen to be almost identical to the 1D analytical model.

As a consequence, the authors believe that this hybrid model can be the perfect tool for the following potential applications.

- Design of fuel cell and electrolysers and geometry optimisation
- Optimisation of the thermal management strategies
- Design of performance maximisation controllers
- Degradation analysis and prognosis
- Techno-economic analysis

Finally, future developments of the present study should be focused on the improvement of the coupling: (i) a thorough analysis of the optimal identification of the regression model, including a broad analysis of the required CFD results; (ii) the analysis of alternative approaches to replace the regression model, such as a reduced-order CFD model or a Machine-Learning-based model; and (iii) the extension of the hybridation approach to electrolysers.

Acknowledgment

This publication is part of the research project TED2021-132767A-I00 funded by the Spanish Ministry of Science and Innovation, the research project funded by the Basque Government's ELKARTEK 2022 program under the grant No. KK-2021/00086, and the project 2022-CIEN-000052-01 funded by the Gipuzkoa Provincial Council. The project is also supported by the Basque Government's Research Group Program under the grant No. IT1505-22.

Appendix A. Supplementary data

Supplementary data to this article can be found online at https://doi.org/10.1016/j.ijhydene.2023.06.082.

REFERENCES

[1] IPCC, "Global Warming of 1. 5°C," intergovernmental panel on climate change (IPCC). Tech Rep 2018. 978-92-9169-151-7.
[2] de Bruyn S, Jongsma C, Kampman B, Gorlach B, Thie J-E. Energy-intensive industries-Challenges and opportunities in energy transition, Industry, Research and Energy (ITRE). Policy Department for Economic, Scientific and Quality of Life Policies, European Parliament, Luxemburg, Tech. Rep.; 2020 [Online]. Available: https://www.europarl.europa.eu/RegData/etudes/STUD/2020/652717/IPOL_STU(2020)652717_EN.pdf.
[3] Prewitz M, Bardenhagen A, Beck R. Hydrogen as the fuel of the future in aircrafts – challenges and opportunities. Int J Hydrogen Energy 2020;45.
[4] Baroutaji A, Wilberforce T, Ramadan M, Olabi AG. "Comprehensive investigation on hydrogen and fuel cell technology in the aviation and aerospace sectors,". Renew Sustain Energy Rev 2019;106.
[5] IRENA. Global energy transformation: a roadmap to 2050. International Renewable Energy Agency, Abu Dhabi, Tech. Rep.; 2019.
[6] Zeng K, Zhang D. Recent progress in alkaline water electrolysis for hydrogen production and applications. Prog Energy Combust Sci 2010;36(3):307–26 [Online]. Available: https://www.sciencedirect.com/science/article/pii/S0360128509000598.
[7] Guo Y, Li G, Zhou J, Liu Y. Comparison between hydrogen production by alkaline water electrolysis and hydrogen production by PEM electrolysis. IOP Conf Ser Earth Environ Sci 2019;371(4).
[8] Escobar-Yonoff R, Maestre-Cambronel D, Charry S, Rincon-Montenegro A, Portnoy I. Performance assessment and economic perspectives of integrated PEM fuel cell and PEM electrolyzer for electric power generation. Heliyon 2021;7(3).
[9] Schröder M, Becker F, Kallo J, Gentner C. Optimal operating conditions of pem fuel cells in commercial aircraft. Int J Hydrogen Energy 2021;46(66).
[10] Tawalbeh M, Alarab S, Al-Othman A, Javed RMN. The operating parameters, structural composition, and fuel sustainability aspects of pem fuel cells: a mini review. Fuel 2022;3(3).
[11] Fernandes M, Andrade S de P, Bistritzki V, Fonseca R, Zacarias L, Gonçalves H, de Castro A, Domingues R, Matencio T. Sofc-apu systems for aircraft: a review. Int J Hydrogen Energy 2018;43(33).
[12] IRENA. Green hydrogen cost reduction: scaling up electrolysers to meet the 1.5°C climate goal. Rep. Abu Dhabi, Tech: International Renewable Energy Agency; 2020 [Online]. Available: /publications/2020/Dec/Green-hydrogen-cost-reduction%0Ahttps://www.irena.org/-/media/Files/IRENA/Agency/Publication/2020/Dec/IRENA_Green_hydrogen_cost_2020.pdf
[13] Yonoff RE, Ochoa GV, Cardenas-Escorcia Y, Silva-Ortega JI, Meriño-Stand L. Research trends in proton exchange membrane fuel cells during 2008–2018: a bibliometric analysis. Heliyon 2019;5(5):e01724 [Online]. Available: https://www.sciencedirect.com/science/article/pii/S2405844018345407.
[14] Andersson M, Beale S, Espinoza M, Wu Z, Lehnert W. A review of cell-scale multiphase flow modeling, including water management, in polymer electrolyte fuel cells. Appl Energy 2016;180:757–78 [Online]. Available: https://www.sciencedirect.com/science/article/pii/S0306261916310972.
[15] Baroutaji A, Arjunan A, Ramadan M, Robinson J, Alaswad A, Abdelkareem MA, Olabi A-G. Advancements and prospects of thermal management and waste heat recovery of PEMFC. International Journal of Thermofluids 2021;9:100064 [Online]. Available: https://www.sciencedirect.com/science/article/pii/S2666202721000021.
[16] Falcao D, Gomes P, Oliveira V, Pinho C, Pinto A. 1D and 3D numerical simulations in PEM fuel cells. Int J Hydrogen Energy 2011;36(19):12486–98 [Online]. Available: https://www.sciencedirect.com/science/article/pii/S0360319911016053 [Online]. Available:.
[17] Zhongliang Li LX, Zheng Zhixue, Lu X. A review of the applications of fuel cells in microgrids: opportunities and challenges. BMC Energy 2019;1(8).
[18] Lazar AL, Konradt SC, Rottengruber H. Open-source dynamic MATLAb/Simulink 1D proton exchange membrane fuel cell model. Energies 2019;12(18).
[19] Abdin Z, Webb CJ, Gray EMA. PEM fuel cell model and simulation in Matlab–Simulink based on physical parameters. Energy 2016;116:1131–44. https://doi.org/10.1016/j.energy.2016.10.033 [Online]. Available:.
[20] Hoeflinger J, Hofmann P. Air mass flow and pressure optimisation of a PEM fuel cell range extender system. Int J Hydrogen Energy 2020;45(53):29246–58. https://doi.org/10.1016/j.ijhydene.2020.07.176 [Online]. Available:.
[21] Zhang C, Li W, Hu M, Cheng X, He K, Mao L. A comparative study of using polarization curve models in proton exchange membrane fuel cell degradation analysis. Energies 2020;13(15).

[22] Yigit T, Selamet OF. Mathematical modeling and dynamic Simulink simulation of high-pressure PEM electrolyzer system. Int J Hydrogen Energy 2016;41(32):13 901–913 914. https://doi.org/10.1016/j.ijhydene.2016.06.022 [Online]. Available:.
[23] Espinosa-López M, Darras C, Poggi P, Glises R, Baucour P, Rakotondrainibe A, Besse S, Serre-Combe P. Modelling and experimental validation of a 46 kW PEM high pressure water electrolyzer. Renew Energy 2018;119:160–73.
[24] Le AD, Zhou B. A general model of proton exchange membrane fuel cell. J Power Sources 2008;182(1):197–222 [Online]. Available: https://www.sciencedirect.com/science/article/pii/S0378775308006083.
[25] Fundamental understanding of liquid water effects on the performance of a pemfc with serpentine-parallel channels. Electrochim Acta 2009;54(8):2137–54 [Online]. Available: https://www.sciencedirect.com/science/article/pii/S0013468608012310.
[26] A generalized numerical model for liquid water in a proton exchange membrane fuel cell with interdigitated design. J Power Sources 2009;193(2):665–83 [Online]. Available: https://www.sciencedirect.com/science/article/pii/S0378775309006442.
[27] A numerical investigation on multi-phase transport phenomena in a proton exchange membrane fuel cell stack. J Power Sources 2010;195(16):5278–91 [Online]. Available: https://www.sciencedirect.com/science/article/pii/S0378775310004040.
[28] Chen L, Cao T-F, Li Z-H, He Y-L, Tao W-Q. Numerical investigation of liquid water distribution in the cathode side of proton exchange membrane fuel cell and its effects on cell performance. Int J Hydrogen Energy 2012;37(11):9155–70 [Online]. Available: https://www.sciencedirect.com/science/article/pii/S0360319912001978.
[29] Tafel J, Emmert B. The cause of the spontaneous depression of cathode potential during the electrolysis of dilute sulphuric acid. Zeitschrift fuer Physikalische Chemie, Stoechiometrie und Verwandtschaftslehre 1905;52:349–73.
[30] Ferreira RB, Falcão D, Oliveira V, Pinto A. Numerical simulations of two-phase flow in proton exchange membrane fuel cells using the volume of fluid method – a review. J Power Sources 2015;277:329–42 [Online]. Available: https://www.sciencedirect.com/science/article/pii/S0378775314019818.
[31] Bednarek T, Tsotridis G. Inter-laboratory comparison of computational fluid dynamics codes for PEM fuel cell modelling, joint research centre, European commission. Luxemburg, Tech. Rep. 2021.
[32] Toghyani S, Afshari E, Baniasadi E, Atyabi SA, Naterer GF. Thermal and electrochemical performance assessment of a high temperature PEM electrolyzer. Energy 2018;152:237–46. https://doi.org/10.1016/j.energy.2018.03.140 [Online].
[33] Ferreira RB, Falcão D, Oliveira V, Pinto A. 1d+3d two-phase flow numerical model of a proton exchange membrane fuel cell. Appl Energy 2017;203:474–95 [Online]. Available: https://www.sciencedirect.com/science/article/pii/S0306261917307997.
[34] Ding Y, Bi X, Wilkinson DP. 3d simulations of the impact of two-phase flow on pem fuel cell performance. Chem Eng Sci 2013;100:445–55. 11th International Conference on Gas-Liquid and Gas-Liquid-Solid Reactor Engineering. [Online]. Available: https://www.sciencedirect.com/science/article/pii/S0009250912006537.
[35] Ding Y, Anderson R, Zhang L, Bi X, Wilkinson DP. Simulations of two-phase flow distribution in communicating parallel channels for a pem fuel cell. Int J Multiphas Flow 2013;52:35–45 [Online]. Available: https://www.sciencedirect.com/science/article/pii/S0301932212001747.
[36] Springer TE, Zawodzinski TA, Gottesfeld S. Polymer electrolyte fuel cell model. J Electrochem Soc aug 1991;138(8):2334–42. https://doi.org/10.1149/1.2085971 [Online].
[37] Amphlett JC, Baumert RM, Mann RF, Peppley BA, Roberge PR, Harris TJ. Performance modeling of the ballard mark IV solid polymer electrolyte fuel cell: I . mechanistic model development. J Electrochem Soc jan 1995;142(1):1–8. https://doi.org/10.1149/1.2043866 [Online].
[38] Barbir F, editor. *PEM fuel cells. Theory and practice*. Plus 0.5em minus 0. 4emELSEVIER; 2013.
[39] J.M. C, F.A. F, L.N. C, M.G. S. An electrochemical-based fuel-cell model suitable for electrical engineering automation approach. IEEE Trans Ind Electron 2004;51(5):1103–12. cited by: 450. [Online]. Available: https://www.scopus.com/inward/record.uri?eid=2-s2.0-5444249240&doi=10.1109%2fTIE.2004.834972&partnerID=40&md5=368a6566cef808a9327371a635a94610.
[40] Biaku C, Dale N, Mann M, Salehfar H, Peters A, Han T. A semiempirical study of the temperature dependence of the anode charge transfer coefficient of a 6kw pem electrolyzer. Int J Hydrogen Energy 2008;33(16):4247–54 [Online]. Available: https://www.sciencedirect.com/science/article/pii/S0360319908007118.
[41] Rosén T, Eller J, Kang J, Prasianakis NI, Mantzaras J, Büchi FN. Saturation dependent effective transport properties of PEFC gas diffusion layers. J Electrochem Soc 2012;159(9):F536–44. https://doi.org/10.1149/2.005209jes [Online]. Available:.
[42] Bird RB. Transport phenomena. Appl Mech Rev 2002;55(1):R1–4. https://doi.org/10.1115/1.1424298 [Online].
[43] Zawodzinski TA, Derouin C, Radzinski S, Sherman RJ, Smith VT, Springer TE, Gottesfeld S. Water uptake by and transport through nafion® 117 membranes. J Electrochem Soc apr 1993;140(4):1041–7. https://doi.org/10.1149/1.2056194 [Online].
[44] Dutta S, Shimpalee S, Van Zee J. Numerical prediction of mass-exchange between cathode and anode channels in a pem fuel cell. Int J Heat Mass Tran 2001;44(11):2029–42 [Online]. Available: https://www.sciencedirect.com/science/article/pii/S001793100000257X.
[45] Mittelsteadt CK, Staser J. Simultaneous water uptake, diffusivity and permeability measurement of perfluorinated sulfonic acid polymer electrolyte membranes. ECS Trans oct 2011;41(1):101–21. https://doi.org/10.1149/1.3635547 [Online].
[46] Carcadea E, Ismail MS, Ingham DB, Patularu L, Schitea D, Marinoiu A, Ion-Ebrasu D, Mocanu D, Varlam M. Effects of geometrical dimensions of flow channels of a large-active-area PEM fuel cell: a CFD study. Int J Hydrogen Energy 2021;46(25).